Supplementary Information

Supplementary Figures S1-S10

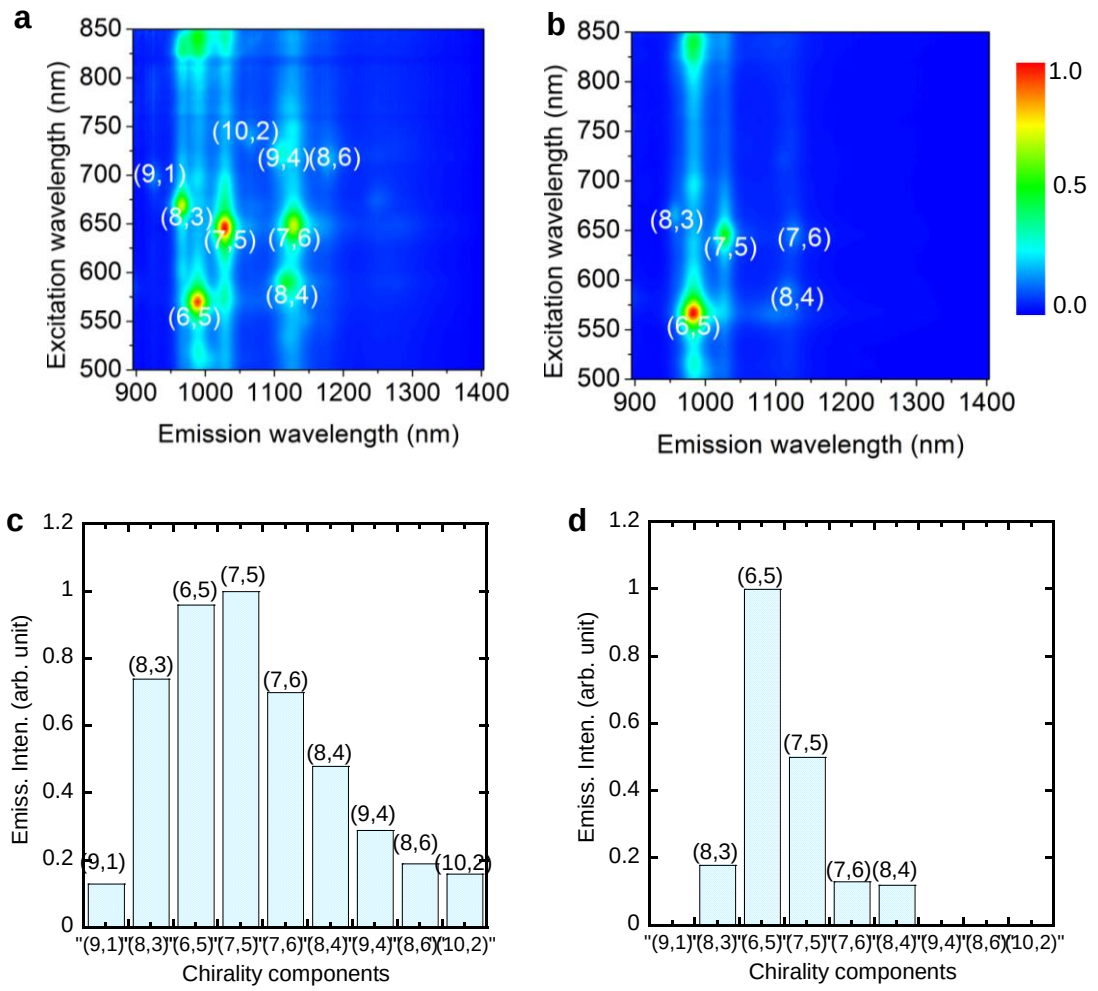

Supplementary Figure S1.

Photoluminescence (PL) maps and the corresponding emission intensity distribution of the selectively adsorbed nanotubes.

a and **c,** the loading amount: 1 ml SWCNT dispersion. **b** and **d,** the loading amount: 8 ml SWCNT dispersion. With an increase in the loading amount of SWCNT dispersion, the chiraity distribution of the adsorbed nanotubes becomes much narrower, indicating the selective adsorption of semiconducting nanotubes was enhanced greatly.

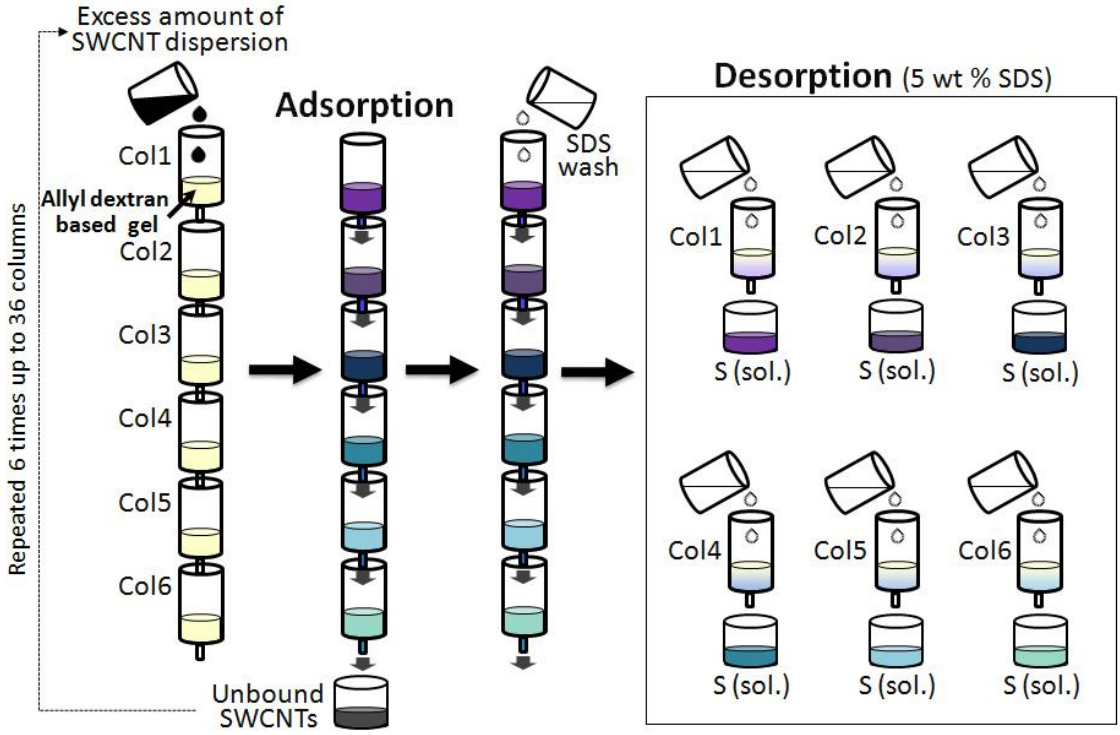

Supplementary Figure S2.

Schematic diagram of single-surfactant multicolumn gel chromatography (SS-MUGEC).

Several gel columns were connected in a vertical row. SWCNT dispersion was applied onto the top column and then a 2 wt% SDS aqueous solution was added to elute unbound nanotubes. Unbound SWCNTs flowed from one column to another under gravity and were finally collected from the bottom column. The trapped semiconducting nanotubes were desorbed and collected from each column by disconnecting the gel column series and adding SDS aqueous solution of 5 wt % respectively. After the equilibration of gel columns with 2 wt % SDS aqueous solution, we repeated the above procedure by loading the unbound SWCNTs until no semiconducting SWCNTs could be trapped in the gel columns. The finally unbound nanotubes were identified as highly metal-enriched nanotubes.

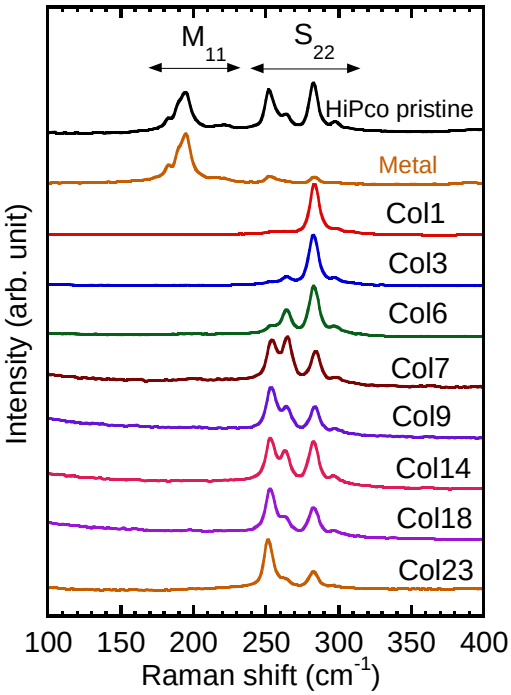

Supplementary Figure S3.

Raman spectra of the separated M- and S-SWCNT fractions in the first separation.

Raman spectra were measured using 633 nm laser excitation. The Raman spectrum of the M-SWCNT fraction contains relatively intense metallic peaks and weak semiconducting peaks. In contrast, the semiconducting peaks are strongly enhanced, whereas the metallic peaks are absent for the S-SWCNT fractions. Since Raman frequency in radial breathing mode (RBM) region of Raman spectra is inversely proportional to a nanotube diameter, semiconducting peaks shifting toward smaller Raman frequency indicate that the nanotube diameter of the S-SWCNT fractions gradually increases from the first column to the last column. (Col: column).

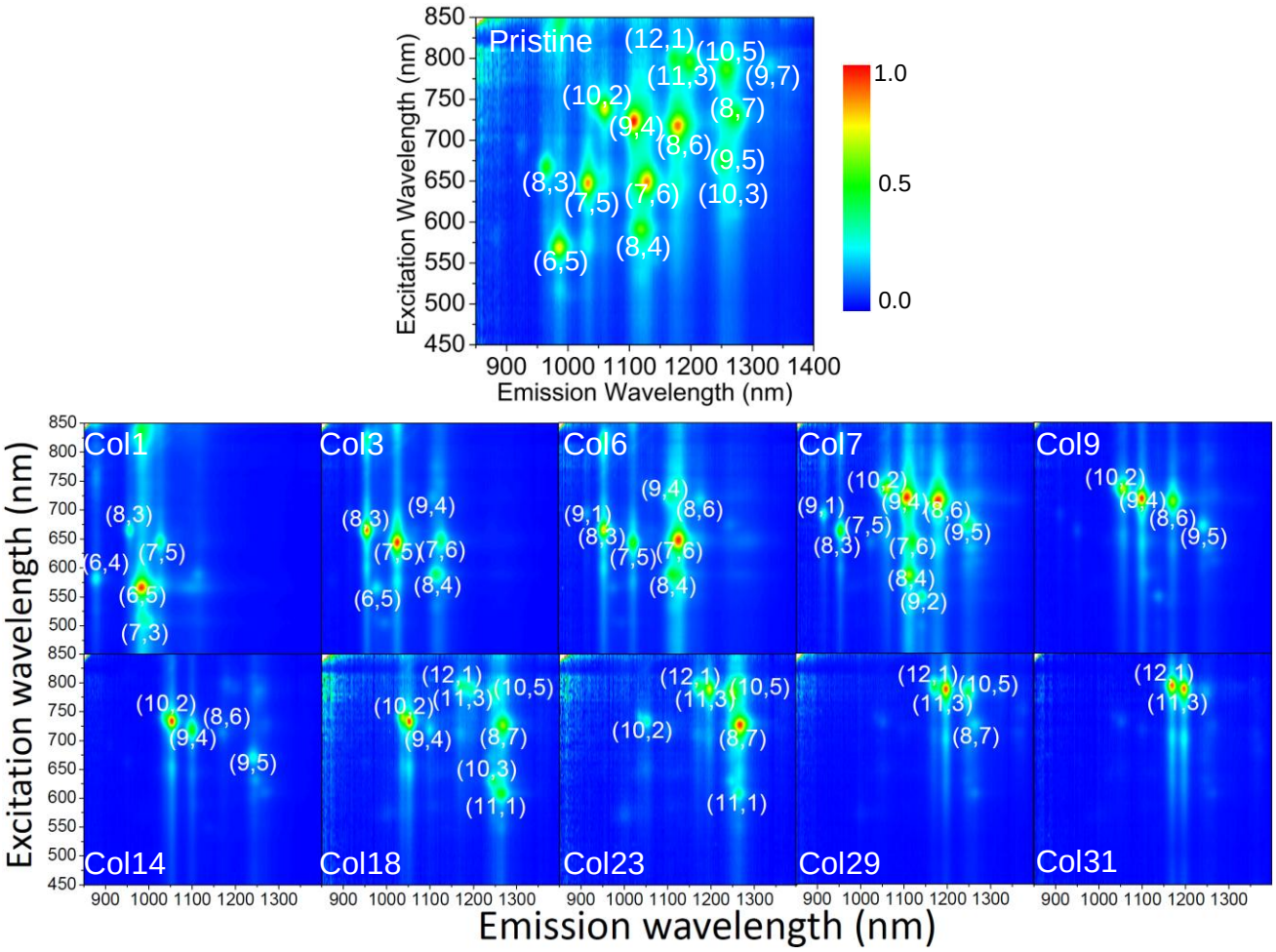

Supplementary Figure S4.

Normalized photoluminescence (PL) contours for the sorted semiconducting fractions in the first separation.

The pristine samples show around 15 semiconducting species, whereas each semiconducting fraction eluted from different columns shows a much narrower chirality distribution. Col is the abbreviation of column. The numbers represent the corresponding gel columns.

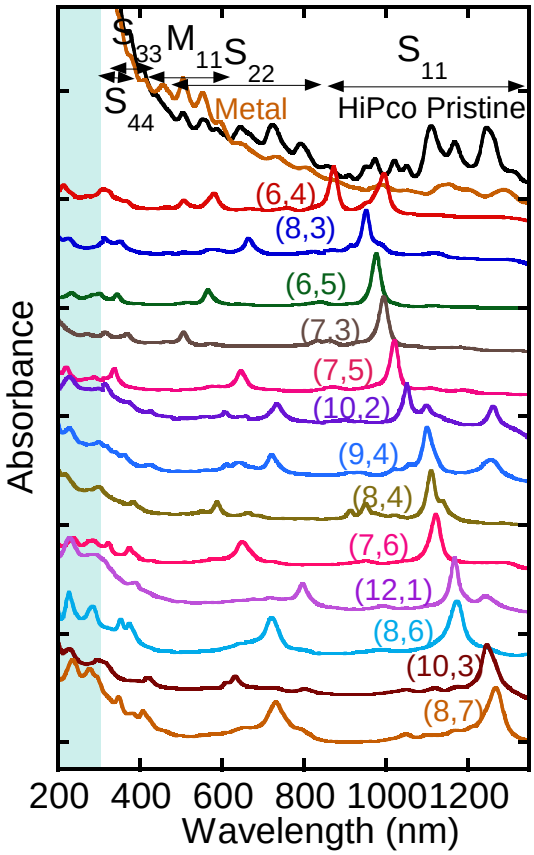

Supplementary Figure S5.

Optical absorption spectra of 13 (*n, m*) semiconducting species, along with separated M-SWCNTs and HiPco (pristine) mixture.

The absorption peaks around 850-1350, 500-850, 330-450, and 300-400 nm derive from first (S_{11}), second (S_{22}), third (S_{33}) and fourth (S_{44}) optical transitions of semiconducting SWCNTs, respectively. The absorbance peak around 400-650 nm represents the first optical transition of metallic SWCNTs (M_{11}). At shorter wavelength (200-300 nm, blue shadow), the blue shaded region shows the ultraviolet optical absorption feature of the nanotubes. The spectra are ranked according to the measured S_{11} absorption wavelength.

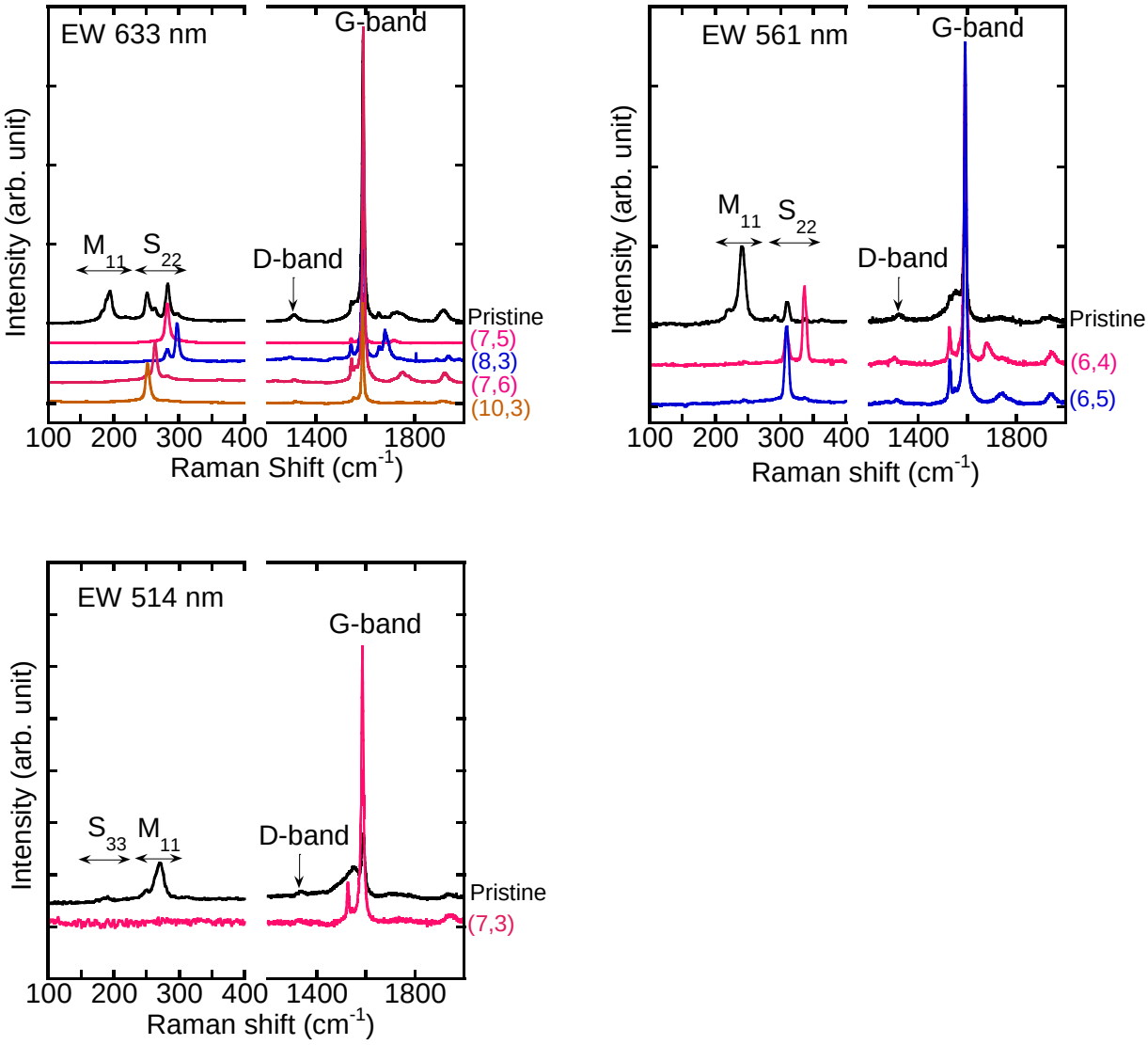

Supplementary Figure S6.

Raman spectra of the separated (*n, m*) nanotubes, along with pristine HiPco mixture.

Different (*n, m*) species were measured respectively by 633, 561 and 514 nm excitation wavelengths because of strong resonance selection of Raman spectroscopy. For each (*n, m*) single-chirality fraction, metallic peaks were not observed, confirming high electronic purity of the separated (*n, m*) tubes. The very low relative D bands of Raman spectra suggest minimal defects in these SS-MUGEC sorted nanotubes.

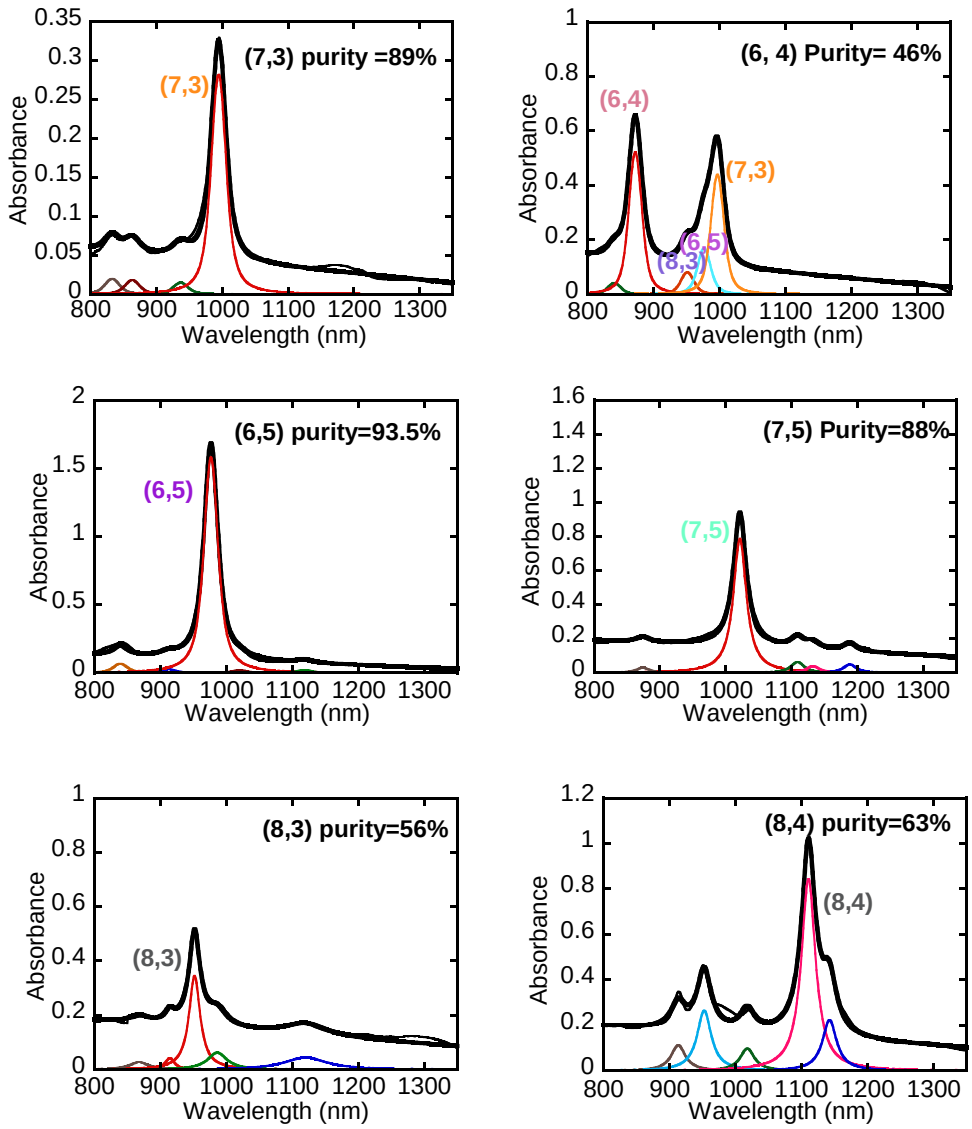

Supplementary Figure S7.

Purity evaluation of the separated (*n, m*) nanotubes using near-IR absorption spectra and spectral simulations.

The PeakFit software was used to simulate each spectrum. The purity of each (n, m) fraction was computed as the ratio of the area of the dominant peak to the sum of the peak areas.

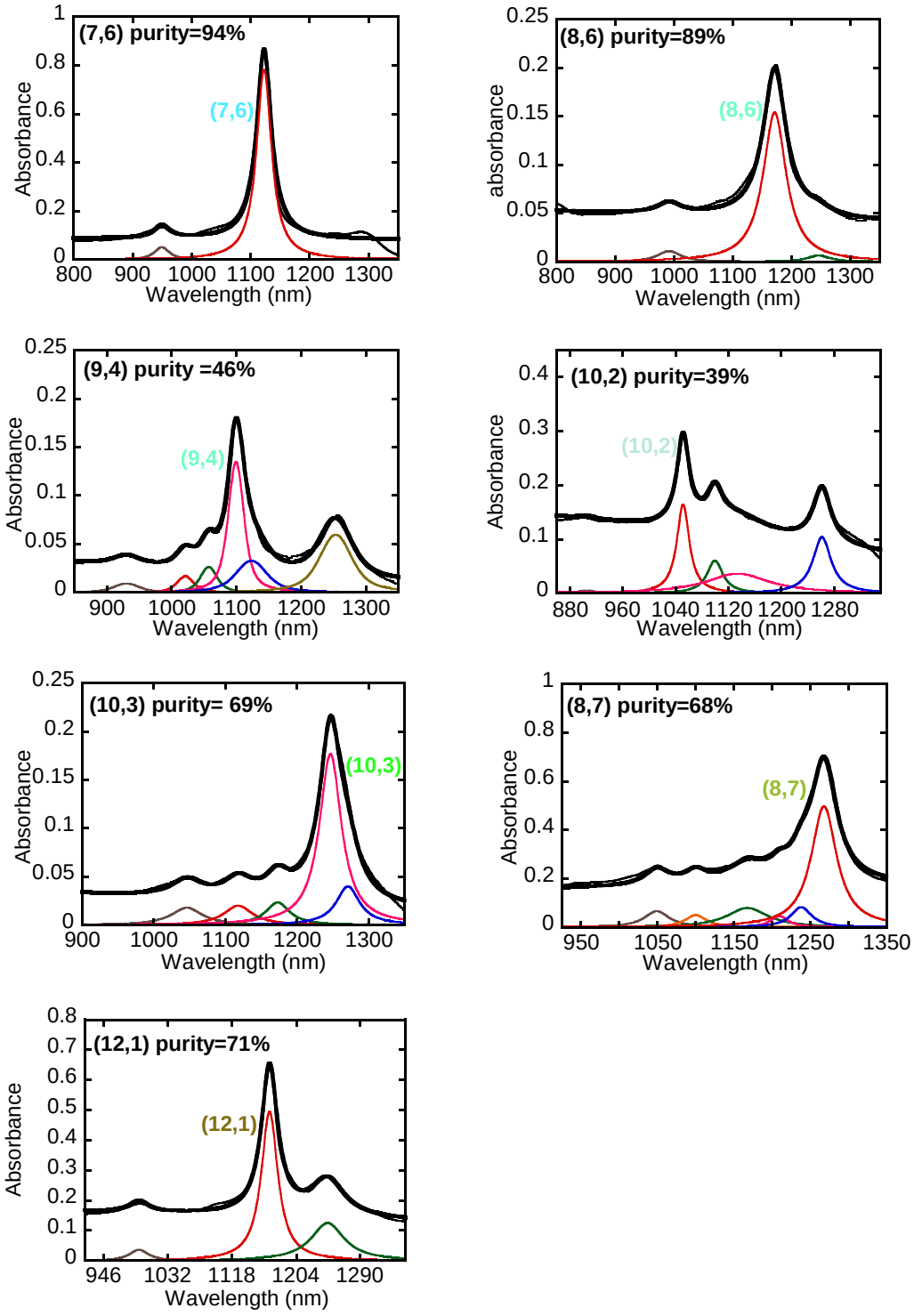

Supplementary Figure S8.

Purity evaluation of the separated (*n, m*) nanotubes using near-IR absorption spectra and spectral simulations (as in Figure S7).

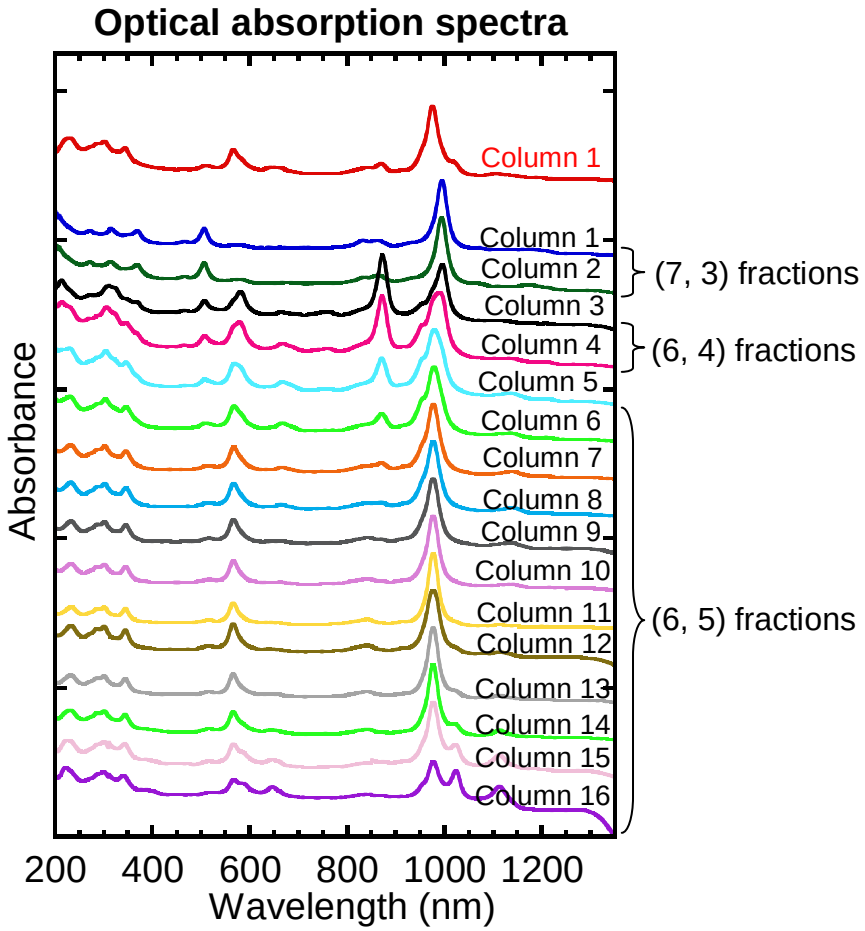

Supplementary Figure S9.

Optical absorption spectra for the sorted S-SWCNT fractions from a semiconducting mixture fraction collected in the first separation.

The top spectrum corresponds to the semiconducting fraction collected from column 1 in the first separation. The lower spectra represent the optical absorbance of the corresponding second separated S-SWCNT fractions, which are indicated with column number in the second separation. In the second separation, we obtained two (7, 3) fractions, two (6, 4) fractions and twelve (6, 5) fractions. It is clear that these (*n, m*)-enriched fractions have different purity degree. The purification yield of each (*n, m*) species depends on their purity degree. The lower the purity is, the higher the purification yield is.

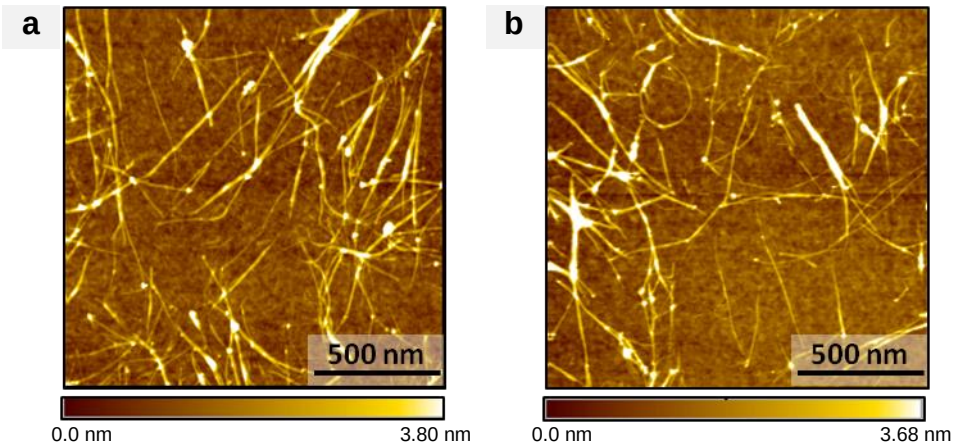

Supplementary Figure S10.

Atomic Force Microscopy (AFM) observation of the separated (6, 5) and (10, 2) nanotubes.

a, (6, 5) nanotube image. **b,** (10, 2) nanotube image. (6, 5) and (10, 2) nanotubes have no clear difference in their morphologies.